

Effects of Mn ions on structural and Mössbauer properties of nanoferrites $\text{Zn}_{1-x}\text{Mn}_x\text{Fe}_2\text{O}_4$ by sol-gel combustion method

Hu Yang¹, Zeping Guo¹, Hui Li¹, Hangyu Xu¹, Yanbing He¹, Henian Chen², Qing Lin^{1,2,a} and Yun He^{1,b}

¹College of Physics and Technology, Guangxi Normal University, Guilin 541004, China

²College of Medical Informatics, Hainan Medical University, Haikou 571199, China

Keywords: Mn ions, structural and Mössbauer properties, sol-gel combustion method

Abstract. $\text{Zn}_{1-x}\text{Mn}_x\text{Fe}_2\text{O}_4$ ($x=0, 0.15, 0.25, 0.35, 0.45, 0.55, 0.75, 0.85$) ferrites were synthesized by sol-gel combustion method with citric acid as complexing agent, and mole ratio of metal ions and citric acid is 1:1. All samples were sintered by 550°C. The structural and magnetic properties of MnZn ferrites were studied. The XRD analysis shows that the structure of samples are cubic spinel ferrite. The SEM analysis shows the samples particles are sphere and agglomeration. The Mössbauer Spectrum analysis shows that the paramagnetic double lines spectra gradually change Zeeman six lines spectra.

Introduction

At present, Mn-Zn ferrites are one of functional materials having relatively active area of research, because Mn-Zn ferrites crucial soft magnetic materials for used storage devices, transformer core, switching devices, electric inductance core[1-4] and so on. However, the microstructural and magnetic properties of Mn-Zn ferrites were influenced by difference of synthesis methods, ions ratio, pH value, complexing agent and calcination temperature[5-8]. R. Gimenes etc [6] studied the microstructure and magnetic properties of Mn-Zn ferrites by citrate precursor method, that it was showed that mean crystallite size and saturation magnetization increased gradually with with the continuous increasing of Mn^{2+} ions concentration. Jun Wang etc [7] reported the structure and magnetic properties of $\text{Mn}_x\text{Zn}_{1-x}\text{Fe}_2\text{O}_4$ nanoparticles, whose research results showed that saturation magnetization increased gradually with with the continuous increasing of Mn^{2+} ions concentration. The composites with the ferrite composition $x=0.2$ are found to show higher reflection loss compared with the composites with other compositions. M. M. Hessien etc[9] synthesized Mn-Zn ferrites by solid reaction process, that their research results showed that ferrites were single spinel ferrite structure by 1200-1300°C sintered, particles size increased with sintered temperature. S.A.Seyyed Ebrahimi etc[10] reported effects of pH and citric acid content on the structure and magnetic properties of Mn-Zn ferrites, whose research results showed that that the single phase Mn-Zn ferrite could be achieved directly without any post-calcination using pH of 7 and CA/MN molar ratio of 0.5, MnZn ferrite nanoparticles prepared by pH=7 and CA/MN=0.5 with the crystallite size of 39 nm exhibited saturation magnetization of 20.9 emu/g and coercivity of 44 Oe. A.C.F.M.Costa etc[11] effect of urea and glycine as complexing agent synthesis of Mn-Zn ferrites, and results showed the saturation magnetization was larger with glycine as complexing agent.

In this paper $\text{Zn}_{1-x}\text{Mn}_x\text{Fe}_2\text{O}_4$ ($x=0, 0.15, 0.25, 0.35, 0.45, 0.55, 0.75, 0.85$) ferrites were synthesized by sol-gel combustion method using citric acid as complexing agent. The aim of this study is to investigate the structural and magnetic properties of ferrite powders by doping small amounts.

Experimental

Sample preparation

The desired proportions of high-purity (AR grade) iron, zine, manganese nitrates and citric acid were weighed and dissolved in distilled water of 80ml. Mole ratio of metal ions and citric acid is 1:1. Ammonia was dropped to control the pH=7 of the mixed solution. The solution was stirred continuously with motor stirrer to form a homogeneous solution at 80°C until the water evaporated to

abtain wet gel . Wet gel were dried at 120°C in a drying oven at 12 hours to form dried gel, being ignited in air at room temperature ,the dried gel burnt in a self-propagating combustion way to form loose powders. All samples were sintered by 550°C to obtain nanosize particles.

Characterizations

The thermal decomposition behavior of gel was analyzed by thermal analysis instrument (SDT Q600, America). The crystalline structure of sample was performed using X-ray diffraction (D8 Advance, Germany) with Cu K α radiation ($\lambda=0.15405\text{nm}$). The microstructure of particles was observed by scanning electron microscope (SU8020, Japan). The Mössbauer spectra were performed using conventional Mössbauer spectrometer (Fast Com Tec PC-moss II) at room temperature, in constant acceleration modeat. The γ -ray was provided by a ^{57}Co source in a rhodium matrix.

Results and discussion

XRD analysis

At room temperature(300k), all datum of the samples were fitted by JADE 5. As shown in Figure 1, the structure of samples are cubic spinel ferrite, main diffractions peak of (220), (311), (222), (400), (422), (511), (440) were observed. The samples were single cubic spinel ferrite, and no impurity phase was detected for $x=0, 0.15, 0.25, 0.35, 0.45, 0.55$. However, for $x=0.75, 0.85$, the samples impurities phases was detected, and impurities were phases of Fe_2O_3 and Mn_2O_3 , because sintering in aerobic environment the number of phases of Fe_2O_3 increased continuously with with the continuous increasing of Mn^{2+} ions concentration[6], as well as it is possible that the decomposition reaction of ferrites happened[12] as follow: $\text{MnFe}_2\text{O}_4 + [\text{O}] \rightarrow \text{Fe}_2\text{O}_3 + \text{Mn}_2\text{O}_3$. The grain size was calculated by Scherrer`s formula[13]: $D = (0.9\lambda) / (\beta \cos \theta)$. Where D is average grain size, λ is the wavelength of copper (0.15405nm), and β is full width at half maximum(FWHM) of the main (311) peak, and θ is Bragg diffraction angle. All the XRD datum listed in table 1. With the continuous increasing of Mn^{2+} ions concentration, the grain size increased, and is about 8.3nm to 14.8nm.

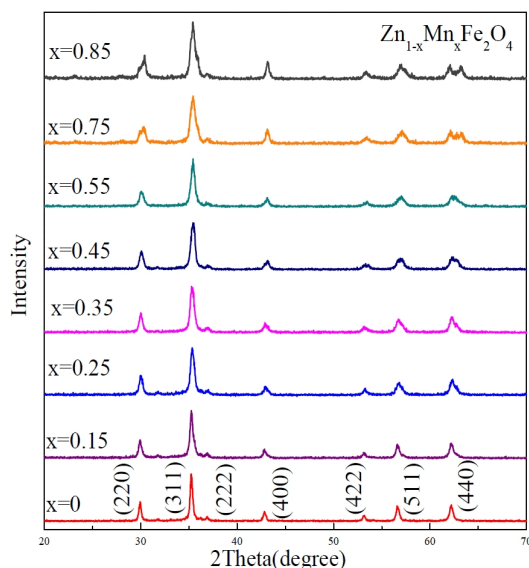


Figure 1. The XRD patterns of samples

The lattice constant is obtained by the following formula: $a = d_{hkl} \sqrt{h^2 + k^2 + l^2}$.Where (hkl) is Miller index, d is crystal plane spacing. With the continuous increasing of Mn^{2+} ions concentration, the lattice constant gradually increased, and this result is consistent with the previous mentioned[14-16], because the ionic radius of Mn^{2+} (0.91Å) are larger than the ionic radii of Zn^{2+} (0.82Å). The figure 2 shown, a obvious displacement of the peak position to smaller angles is observed for the (311) reflection peak, indicating a decrease in the lattice parameter.

The density of X-Ray decreased with the continuous increasing of Mn^{2+} ions concentration. The density of X-Ray depends on the lattice constants and the molar mass of the sample[15]. It can be

determined by the following formula: $\rho_x = \frac{8M}{Na^3}$. Where M and N is the molar mass of sample and Avogadro constant, respectively, and a is the lattice constant. Because the molar mass of sample decreased, and the lattice constant increased, the density of X-Ray decreased.

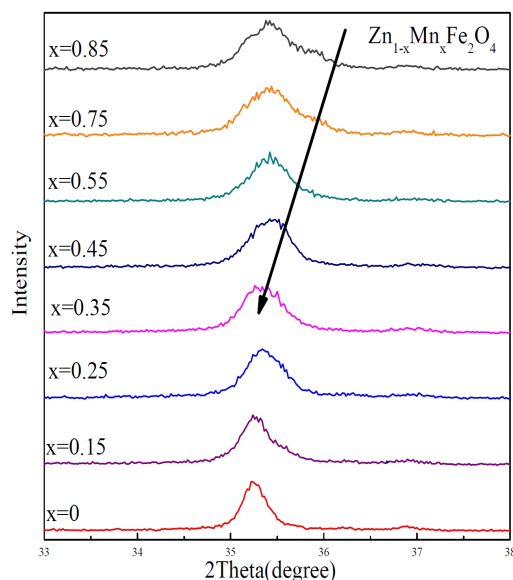


Figure 2. The (311) peak of samples enlarge figure

Table 1. The XRD datum of $Zn_{1-x}Mn_xFe_2O_4$ samples

Sampl e (x)	Average crystallit e size	Lattice parameter (Å)	Densit y (g·cm ⁻³)
0	148	8.432	5.33
0.15	110	8.432	5.27
0.25	92	8.439	5.25
0.35	101	8.442	5.22
0.45	94	8.449	5.20
0.55	90	8.408	5.26
0.75	83	8.415	5.19
0.85	83	8.404	5.17

SEM analysis

At room temperature(300k), the SEM pictures of $Zn_{0.85}Mn_{0.15}Fe_2O_4$ and $Zn_{0.45}Mn_{0.55}Fe_2O_4$ ferrites as shown in figure 3. It can be seen the particles were spherical, and serious agglomerated, because the samples are magnetic powders particles. Figure 4 shows the grain size distribution of $Zn_{0.85}Mn_{0.15}Fe_2O_4$ and $Zn_{0.45}Mn_{0.55}Fe_2O_4$ ferrites powders. The average grain size of $Zn_{0.85}Mn_{0.15}Fe_2O_4$ and $Zn_{0.45}Mn_{0.55}Fe_2O_4$ ferrites were obtained by a statistical method is about 30.96 nm and 29.53 nm, respectively. The statistical average grain size of SEM picture is larger than crystalline size of XRD. This shows that the samples are polycrystalline ferrites.

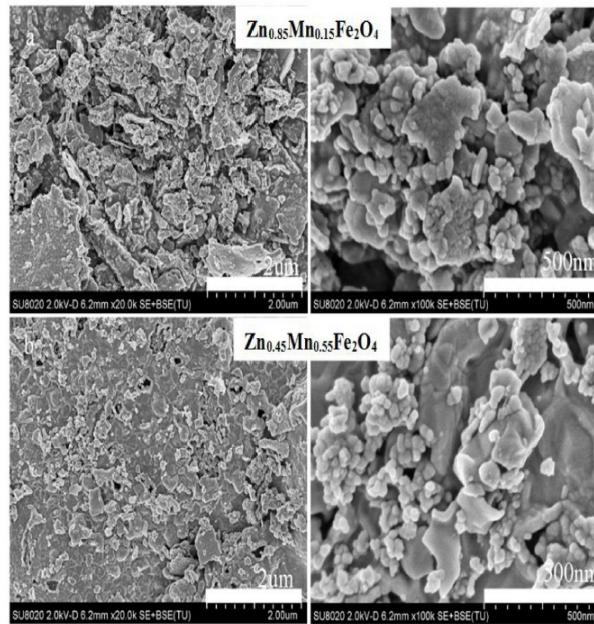


Figure 3. The SEM pictures of $\text{Zn}_{0.85}\text{Mn}_{0.15}\text{Fe}_2\text{O}_4$ and $\text{Zn}_{0.45}\text{Mn}_{0.55}\text{Fe}_2\text{O}_4$

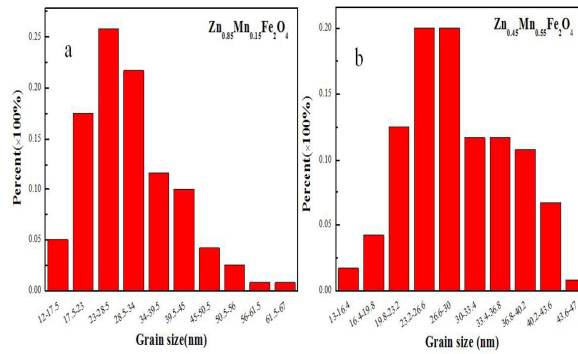


Figure 4. The grain size distribution of $\text{Zn}_{0.85}\text{Mn}_{0.15}\text{Fe}_2\text{O}_4$ and $\text{Zn}_{0.45}\text{Mn}_{0.55}\text{Fe}_2\text{O}_4$ ferrites

Mössbauer spectrum analysis

At room temperature (300K), figure 5 shows the Mössbauer Spectrometer of $\text{Zn}_{1-x}\text{Mn}_x\text{Fe}_2\text{O}_4$ ferrites are fitted by Mosswin 3.0, and all the datum listed in table 2. The spectra of the samples for $x=0.0$ and 0.1 were fitted by a set of paramagnetic double line. For $x=0.25, 0.35, 0.45$ and 0.55 , the spectra of the samples were fitted by a set of zeeman six line and a set of paramagnetic double line. For $x=0.75$, the spectra of the samples were fitted by two sets of zeeman six line and a set of paramagnetic double line. For $x=0.85$, the spectra of the samples were fitted by two sets of zeeman six line. The paramagnetic double lines spectra gradually change zeeman six lines spectra, and this shows that with Mn^{2+} ions concentration increasing the paramagnetic phase gradually transformed into a ferromagnetic phase.

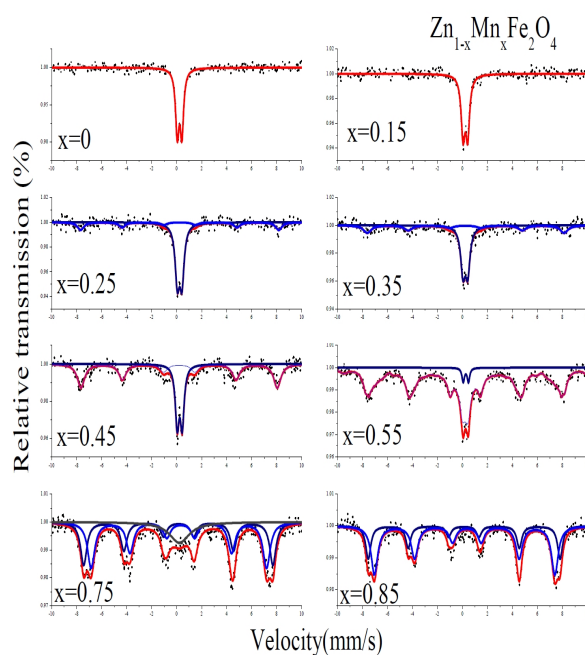


Figure 5. Mössbauer Spectrometer of $\text{Zn}_{1-x}\text{Mn}_x\text{Fe}_2\text{O}_4$ ferrites

Table 2. The Mössbauer spectra of $\text{Zn}_{1-x}\text{Mn}_x\text{Fe}_2\text{O}_4$

Sample (x)	IS (mm/s)	QS (mm/s)	Γ (mm/s)	A_0 (%)
0	0.23	0.37	0.33	100
0.15	0.23	0.37	0.36	100
0.25	0.23	0.36	0.42	63.4
	0.23	0.01	0.61	36.6
0.35	0.23	0.36	0.44	63.4
	0.24	0.01	0.75	36.6
0.45	0.24	0.39	0.36	39.2
	0.21	-0.01	0.69	60.8
0.55	0.26	0.42	0.23	3.2
	0.21	-0.01	0.32	96.8
0.75	0.21	0	1.35	14.9
	0.14	-0.03	0.61	38.6
	0.24	0.15	0.69	46.5
0.85	0.12	0.03	0.49	34.0
	0.26	-0.17	0.64	66.0

The paramagnetic phase exists because the surrounding of the part of iron ions have the nearest disordered spin magnetic moment, and the existence of Zeeman six line magnetic pattern due to the superexchange interaction between the magnetic ions at A- and B- sublattices. As we all know that change of isomer shift is connected with s-electron charge density of Fe^{3+} ions, it depends on the change of the electronic density of shielding effect of the s, p and d orbital electron. For two sets of Zeeman six line-spectrum, the two sextets corresponding to Fe^{3+} on A-sites and B-sites respectively in the spinel lattice.

Generally speaking, it is known that isomer shift value for octahedral sites is more than that for

tetrahedral sites, because the bond separation $\text{Fe}^{3+}-\text{O}^{2-}$ is larger for B-site than A-site as the overlapping of orbital of Fe^{3+} ions is large at A-site in cubic spinel ferrites[17,18]. Being known according to the literature[18], the isomer shift is 0.1~0.5 mm/s relative to Fe metal, which indicates that both Fe ions are in Fe^{3+} state. the isomer shift is 0.6~1.7 mm/s relative to Fe metal, which indicates that both Fe ions are in Fe^{2+} state. As seen in table 2, the isomer shift distributed in the 0.14 mm/s to 0.26 mm/s, which indicates that both Fe ions are in Fe^{3+} state. The isomer shift has significant change with Mn^{2+} ions concentration increasing, which shows substitution of Mn^{2+} ions makes little change in the electron density distribution of the s-shell of the iron ion. The quadrupole splitting QS indicates the symmetry of irons' surrounding[19,20]. The quadrupole splitting QS of all samples are both small, which indicates the charge distribution of the nucleus has no slightly change, and keeps symmetry. Line width increases at first and then decreases with Mn^{2+} ions concentration increasing[21]. Because substitution of Mn^{2+} ions can increase the amount of $\text{Mn}^{2+}-\text{Fe}^{3+}$ and $\text{Fe}^{3+}-\text{Fe}^{3+}$ ion pairs leading to change of net magnetic field, Line width changes. In addition, the existence of relaxation effect leads to change of Line width[21].

Conclusions

The samples were single cubic spinel ferrites. With the continuous increasing of Mn^{2+} ions concentration, the grain size increased, and is about 8.3 nm to 14.8 nm. The average grain size of $\text{Zn}_{0.85}\text{Mn}_{0.15}\text{Fe}_2\text{O}_4$ and $\text{Zn}_{0.45}\text{Mn}_{0.55}\text{Fe}_2\text{O}_4$ ferrites were obtained by a statistical method is about 30.96 nm and 29.53 nm, respectively. The statistical average grain size of SEM picture is larger than crystalline size of XRD. This shows that the samples are polycrystalline ferrites. the isomer shift distributed in the 0.14 mm/s to 0.26 mm/s, which indicates that both Fe ions are in Fe^{3+} state. The quadrupole splitting QS of all samples are both small, which indicates the charge distribution of the nucleus has no slightly change, and keeps symmetry.

Acknowledgments

This work was supported by the National Natural Science Foundation of China(NO.11364004, 11164002); Graduate student excellent thesis cultivation plan of Guangxi Normal University (NO.A410213000001).

References

1. L.Nalbandian, A.Delimitis, V.T.Zaspalis, E.A.Deliyanni, D.N.Bakoyannakis, E.N.Peleka. Microporous and Mesoporous Materials, 2008, 114, 465-473.
2. Ott G, Wrba J. Journal of Magnetism and Magnetic Materials, 2003, 535, 254-255.
3. Uzma Ghazanfar, Siddiqi S A, Abbas G. Mater Sci Eng B, 2005, 118, 84-86 .
4. Jing Feng, Li-Qin Guo, Xiaodong Xu, Shu-Yan Qi, Mi-Lin Zhang. Physica B, 2007, 394, 100-103.
5. Andris SUTKA and Gundars MEZINSKIS. Front. Mater. Sci, 2012, 6(2), 128-141.
6. R.Gimenes, M.R.Baldissera, M.R.A.da Silva, C.A.da Silveira, D.A.W.Soares, L.A.Perazolli, M.R.da Silva, M.A.Zaghete. Ceramics International, 2012, 38, 741-746.
7. Jun Wang, Chuan zeng, Zhenmeng Peng, Qianwang Chen. Physica B, 2004, 349, 124-128.
8. Weijie Wang, Chongguang Zang, Qingjie Jiao. Journal of Magnetism and Magnetic Materials, 2014, 349, 116-120.
9. M.M.Hessien, M.M.Rashad, K.El-Barawy, I.A.Ibrahim. Journal of Magnetism and Magnetic Materials, 2008, 320(9), 1615-1621.
10. S.A.Seyyed Ebrahimi, S.M.Masoudpanah. Journal of Magnetism and Magnetic Materials, 2014, 357, 77-81.
11. A.C.F.M.Costa, V.J.Silva, C.C.Xin, D.A.Vieira, D.R.Cornejo, R.H.G.A.Kiminami. Journal of Alloys and Compounds, 2010, 495, 503-505.

12. Hassan Hejase, Saleh S. Hayek, Shahnaz Qadri, Yousef Haik. Journal of Magnetism and Magnetic Materials, 2012, 324, 3620-3628.
13. C.Rath, K.K.Sahu, S.Anand, S.K.Date, N.C.Mishra, R.P.Das. Journal of Magnetism and Magnetic Materials, 1999, 202, 77-84.
14. Ping Hu, Hai-bo Yang, De-an Pan, Hua Wang, Jian jun Tian, Shen gen Zhang. Journal of Magnetism and Magnetic Materials, 2010, 322, 173-177.
15. P.P.Hankare, R.P.Patil, U.B.Sankpal, S.D.Jadhav, K.M.Garadkar, S.N.Achary. Journal of Alloys and Compounds, 2011, 509, 276-280.
16. Shen Wu, Aizhi Sun, Wenhuan Xu, Qian Zhang, Fuqiang Zhai, Philip Logan, Alex A.Volinsky. Journal of Magnetism and Magnetic Materials, 2012, 324, 3899-3905.
17. Lijun Zhao, Zhaoyang Han, Hua Yang, Lianxiang Yu, Yuming Gui, Weiqun Jin, Shouhua Feng. Journal of Magnetism and Magnetic Materials, 2007, 309, 11-14.
18. S.S.R. Inbanathan, V. Vaithyanathan, J. Arout Chelvane, G. Markandeyulu, K. Kamala Bharathi. Journal of Magnetism and Magnetic Materials, 2014, 353, 41-44.
19. A.D.P. Rao, B. Ranmesh, P.R.M. Rao, S.B. Raju. Journal of Alloys and Compounds, 1999, 282, 268-273.
20. Haining Ji, Zhongwen Lan, Zhiyong Xu, Huaiwu Zhang, and Gregory J. Salamo. IEEE Transactions Magnetism, 2013, 49(7), 4277-4280.
21. U.B. Gawas, V. M. S. Verenkar, S. R. Barman, S. S. Meena, Pramod Bhatt. Journal of Alloys and Compounds, 2013, 555, 225-231.